Signatures of quantum phase transitions in parallel quantum dots: Crossover from local moment to underscreened spin-1 Kondo physics

Arturo Wong, W. Brian Lane, Luis G. G. V. Dias da Silva, Kevin Ingersent, Nancy Sandler, and Sergio E. Ulloa

Phys. Rev. B **85**, 115316 — Published 22 March 2012

DOI: 10.1103/PhysRevB.85.115316

Signatures of quantum phase transitions in parallel quantum dots: Crossover from local-moment to underscreened spin-1 Kondo physics

Arturo Wong,[1,2] W. Brian Lane,[2,3] Luis G. G. V. Dias da Silva,[4]
Kevin Ingersent,[2] Nancy Sandler,[1] and Sergio E. Ulloa[1]

[1]*Department of Physics and Astronomy, Nanoscale and Quantum Phenomena Institute, Ohio University, Athens, Ohio 45701, USA*
[2]*Department of Physics, University of Florida, P.O. Box 118440, Gainesville, Florida 32611, USA*
[3]*Department of Physics, Jacksonville University, 2800 University Boulevard North, Jacksonville, Florida 32211, USA*
[4]*Instituto de Física, Universidade de São Paulo, C.P. 66318, 05315-970 São Paulo, SP, Brazil*

(Dated: March 12, 2012)

We study a strongly interacting "quantum dot 1" and a weakly interacting "dot 2" connected in parallel to metallic leads. Gate voltages can drive the system between Kondo-quenched and non-Kondo free-moment phases separated by Kosterlitz-Thouless quantum phase transitions. Away from the immediate vicinity of the quantum phase transitions, the physical properties retain signatures of first-order transitions found previously to arise when dot 2 is strictly noninteracting. As interactions in dot 2 become stronger relative to the dot-lead coupling, the free moment in the non-Kondo phase evolves smoothly from an isolated spin-one-half in dot 1 to a many-body doublet arising from the incomplete Kondo compensation by the leads of a combined dot spin-one. These limits, which feature very different spin correlations between dot and lead electrons, can be distinguished by weak-bias conductance measurements performed at finite temperatures.

PACS numbers: 72.15.Qm,73.63.Kv,73.23.-b,64.70.Tg

I. INTRODUCTION

Semiconductor quantum dots afford a level of experimental control that has made them the premier setting[1] in which to investigate the Kondo effect, *i.e.*, the many-body screening of a local moment by delocalized electrons. In recent years, interest has turned from Kondo physics in single dots to similar phenomena in more complex structures such as double-dot devices,[2,3] where quantum phase transitions (QPTs) have been predicted[4–10] and possibly observed.[3]

Kondo physics in two spin-degenerate quantum dots (or two levels within a single dot) connected in parallel to the same single-channel leads has been investigated from a number of perspectives. The combined spin of the two localized levels can be tuned between singlet and triplet configurations by adjusting a magnetic field[11] or gate voltages.[12] When coupled to leads, such setups exhibit enhanced conductance near the singlet-triplet level crossing,[12–14] with QPTs of the Kosterlitz-Thouless type.[4,15] Another theme that has received considerable attention is the role of interference between different current paths in modulating the conductance through parallel quantum-dot setups[7,8,16] or pairs of dots embedded in the arms of an Aharanov-Bohm ring.[9,17]

Theoretical studies of parallel double quantum dots have overwhelmingly focused on the limit in which each dot has strong Coulomb interactions and can acquire a magnetic moment. Such systems exhibit two phases[6,10]: a Fermi-liquid phase with a singlet ground state, and a "singular Fermi liquid" phase having a residual spin-$\frac{1}{2}$ arising from an underscreened spin-1 Kondo effect.[18] These phases are separated by lines of Kosterlitz-Thouless QPTs broken by first-order QPTs at points of exact equivalence between the dots.[10]

Parallel doublet dots in a very different limit, where "dot 1" has strong interactions but "dot 2" is strictly noninteracting (and hence nonmagnetic), have been shown[7] to realize the pseudogap Kondo effect,[19,20] in which a magnetic impurity couples to a conduction band having a density of states that vanishes in power-law fashion at the Fermi energy. This reduction of the low-energy density of states inhibits the Kondo effect unless the effective impurity-band exchange coupling exceeds a critical value. The Kondo-screened phase is separated from a non-Kondo local-moment phase by first-order QPTs that exhibit clear signatures in finite-temperature transport.[8]

In this work we explore the connection between limits described in the previous two paragraphs by considering the effect of increasing the dot-2 Coulomb interaction U_2 from zero. A free-moment phase with an unquenched spin-$\frac{1}{2}$ occupies a region of parameter space that grows with U_2 and is separated from a surrounding strong-coupling phase by Kosterlitz-Thouless QPTs. For $U_2 \lesssim \Gamma_2$—the level width of dot 2 due to its coupling to the leads—the properties retain signatures of the $U_2 = 0$ pseudogap Kondo physics, while for $U_2 \gg \Gamma_2$ there is a smooth crossover to the heavily studied limit of two strongly interacting dots. These two regimes, both exhibiting singular Fermi liquid behavior with very different dot-lead entanglements, can be distinguished through weak-bias conductance measurements at experimentally accessible temperatures. In experiments, it is impractical to adjust U_2 by orders of magnitude, but the crossover from $U_2 \ll \Gamma_2$ to $U_2 \gg \Gamma_2$ can be accessed by tuning Γ_2 via gate voltages. The setup therefore has great potential

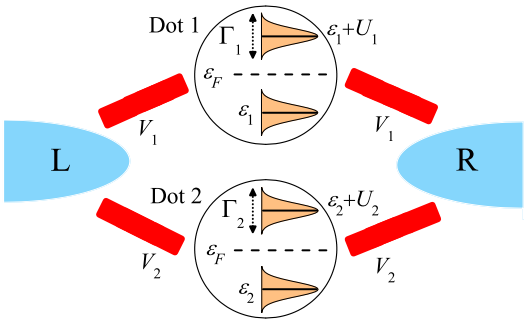

FIG. 1: (Color online) Schematic of the parallel double-quantum-dot setup considered in this work.

for investigation of QPTs and of entanglement in singular Fermi liquids, which lie on the borderline between regular Fermi liquids and non-Fermi liquids.[21]

The double-quantum-dot setup and its phase diagram are described in Sec. II. Section III compares the cases $U_2 = 0$ and $U_2 = \Gamma_2$, the latter typifying the behavior for a weakly correlated dot 2, while Sec. IV addresses the crossover from weak to strong dot-2 interactions. The results are summarized in Sec. V.

II. MODEL AND PHASE DIAGRAMS

We consider an equilibrium system represented schematically in Fig. 1 and modeled by a generalized Anderson Hamiltonian

$$H = H_{\rm leads} + H_{\rm dots} + H_{\rm mix}. \tag{1}$$

Here,

$$H_{\rm leads} = \sum_{j,\mathbf{k},\sigma} \epsilon_{j\mathbf{k}} c^\dagger_{j\mathbf{k}\sigma} c_{j\mathbf{k}\sigma} \tag{2}$$

represents the left (L) and right (R) leads, with $c_{j\mathbf{k}\sigma}$ annihilating an electron in lead j of wave vector $\mathbf{k}$, spin z component σ, and energy $\epsilon_{\mathbf{k}}$;

$$H_{\rm dots} = \sum_{i=1}^{2} \left(\varepsilon_i n_i + U_i n_{i\uparrow} n_{i\downarrow}\right) \tag{3}$$

describes the energetics of the dots in terms of their occupancies $n_{i\sigma} = d^\dagger_{i\sigma} d_{i\sigma}$ and $n_i = n_{i\uparrow} + n_{i\downarrow}$, where $d_{i\sigma}$ annihilates an electron of spin z component σ in the level of dot i that lies closest to the common Fermi energy of the two leads (taken to be $\varepsilon_F = 0$); and

$$H_{\rm mix} = \sum_{i,j,\mathbf{k},\sigma} V_{ij} \left(d^\dagger_{i\sigma} c_{j\mathbf{k}\sigma} + \text{H.c.}\right) \tag{4}$$

accounts for electron tunneling between dots and leads. For simplicity, we take real dot-lead couplings $V_{iL} = V_{iR} \equiv V_i/\sqrt{2}$, for which case the dots interact only with one effective band formed by an even-parity combination of L and R states. We assume a constant density of states $\rho = 1/(2D)$ with half bandwidth D, so that the dot-lead tunneling is measured via the hybridization widths $\Gamma_i = \pi\rho V_i^2$. At low bias, electron transmission described by a Landauer-like formula[22] gives a linear conductance

$$g(T) = \frac{2e^2}{h} \int d\omega \left(\frac{-\partial f}{\partial \omega}\right) \pi \sum_{i,j} \sqrt{\Gamma_i \Gamma_j}\, A_{ij}(\omega, T), \tag{5}$$

where $f(\omega, T) = [\exp(\omega/T) + 1]^{-1}$ is the Fermi-Dirac function and $A_{ij}(\omega, T) = -\pi^{-1} \,\mathrm{Im}\, G_{ij}(\omega, T)$ is the spectral density corresponding to the retarded Green's function $G_{ij}(\omega, T) = -i \int_0^\infty dt e^{i\omega t} \langle\{d_{i,\sigma}(t),\, d^\dagger_{j,\sigma}(0)\}\rangle$.

We have studied this model using the numerical renormalization group[23] with discretization parameter $\Lambda = 2.5$, retaining at least 1000 states after each iteration.[24] This paper focuses on the representative case of a strongly interacting dot 1 described by $U_1 = 10\Gamma_1 = 0.5D$ and a dot-2 hybridization width $\Gamma_2 = 0.02D$. We show the variation of physical properties with temperature T and the dot energies ε_i (which should be experimentally tunable via plunger gate voltages) for different values of U_2. We reiterate that in real devices, U_2 will likely be fixed and Γ_2 instead will be varied by raising or lowering tunnel barriers.

It is instructive first to consider the dots isolated from the leads, *i.e.*, the limit $\Gamma_1 = \Gamma_2 = 0$. Figures 2(a)–2(c) show $T = 0$ occupancies ($\langle n_1\rangle, \langle n_2\rangle$) vs the level energies $\delta_i = \varepsilon_i + \frac{1}{2}U_i$ measured from particle-hole symmetry for three values of the dot-2 Coulomb interaction strength: $U_2 = 0$, $U_2 = 0.02D$ ($\ll U_1$) and $U_2 = 0.5D$ ($= U_1$). The value of $\langle n_i\rangle$ jumps on crossing a dashed line representing $\delta_i = \pm\frac{1}{2}U_i$. For $U_2 = 0$ [Fig. 2(a)], $\langle n_2\rangle = 1$ only when the dot-2 level lies precisely at the chemical potential (along the line $\delta_2 = 0$) and the δ_1-δ_2 plane divides into six two-dimensional regions. For $U_2 > 0$ [Figs. 2(b,c)], there are instead nine regions, including three in which dot 2 is singly occupied and hence carries a magnetic moment.

When both dots are connected to the metallic leads ($\Gamma_1, \Gamma_2 \neq 0$), the numerical renormalization-group solution reveals that most of the δ_1-δ_2 plane is occupied by a *strong-coupling phase* in which all dot degrees of freedom are quenched at $T = 0$. Within this phase, the first-order QPTs present for isolated dots (dashed lines in Fig. 2) are replaced by smooth crossovers between single-particle scattering of lead electrons (wherever each dot is either empty or full, *i.e.*, $|\delta_i| - \frac{1}{2}U_i \gg \Gamma_i$ for $i = 1$ *and* 2) and many-body Kondo physics (wherever one of the dots is singly occupied, *i.e.*, $|\delta_i| - \frac{1}{2}U_i \ll -\Gamma_i$ for $i = 1$ *or* 2). However, the region around the particle-hole-symmetric point $\delta_1 = \delta_2 = 0$ forms a distinct *free-moment phase* in which a spin-$\frac{1}{2}$ degree of freedom survives down to $T = 0$. With increasing U_2, this free-moment phase grows—primarily along the δ_2 axis—as illustrated by the solid lines in Fig. 2.

The next two sections present physical properties along

paths in parameter space that are represented schematically by arrows in Fig. 2. Each path crosses the phase boundary at a location that can be parametrized as $\varepsilon_1 = \varepsilon_1^{\pm}(U_2, \varepsilon_2)$. (This notation suppresses additional dependences of the phase boundaries on U_1 and on the level widths Γ_1 and Γ_2, three quantities that are held constant for all the results presented in this paper.) The Hamiltonian (1) is invariant (up to a constant) under the particle-hole transformation $c_{j\mathbf{k}\sigma} \to c^\dagger_{j\mathbf{k}\sigma}$, $d_{i\sigma} \to -d^\dagger_{i\sigma}$, $\epsilon_{j\mathbf{k}} \to -\epsilon_{j\mathbf{k}}$, and $\delta_i \to -\delta_i$. This symmetry implies that the phase boundaries in Fig. 2 are invariant under a simultaneous change in the sign of δ_1 and δ_2, or equivalently that $\varepsilon_1^-(U_2, \varepsilon_2) = -U_1 - \varepsilon_1^+(U_2, -U_2 - \varepsilon_2)$.

III. ZERO VERSUS WEAK DOT-2 INTERACTIONS

We begin by presenting the properties of the double-quantum-dot system when Coulomb interactions in dot 2 are much weaker than in dot 1. We will focus on two specific cases, namely, $U_2 = 0$ and $U_2 = \Gamma_2$. An understanding of these cases will allow us to establish a connection with the large-U_2 regime in Sec. IV.

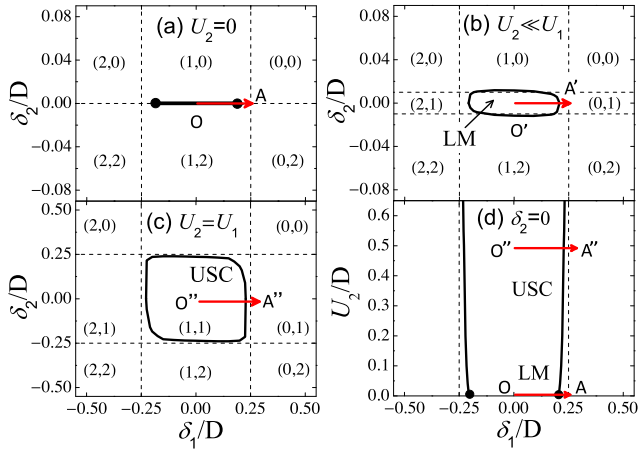

FIG. 2: (Color online). Ground states of the isolated quantum dots [dashed lines and dot occupancies $(\langle n_1\rangle, \langle n_2\rangle)$] and phases of the full system for $\Gamma_1 = 0.05D$, $\Gamma_2 = 0.02D$ (solid lines) vs level energies $\delta_i = \varepsilon_i + \frac{1}{2}U_i$ measured from particle-hole symmetry for (a) $U_2 = 0$, (b) $U_2 = 0.02D \ll U_1$ and (c) $U_2 = U_1$. (d) Phase diagram of the full system on the δ_1-U_2 plane at $\delta_2 = 0$, showing local-moment (LM) and underscreened spin-1 Kondo (USC) regimes within the free-moment phase. Filled circles in (a) and (d) indicate first-order QPTs occurring only for $U_2 = 0$, while all other points along the phase boundaries correspond to QPTs of the Kosterlitz-Thouless type. Arrows represent paths along which data are plotted in Figs. 2–4 and 7.

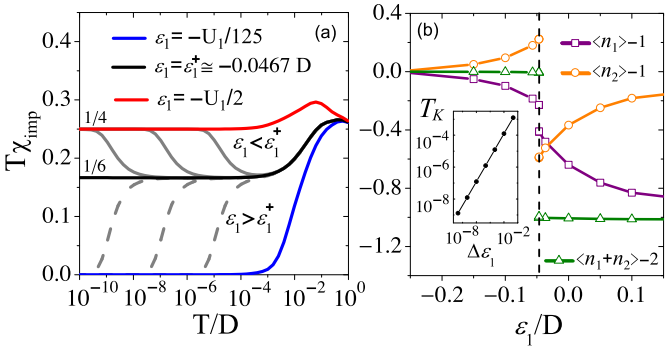

FIG. 3: (Color online). Noninteracting dot 2, $U_2 = \varepsilon_2 = 0$: (a) $T\chi_{\rm imp}$ vs T for various values of ε_1 spanning the QPT at ε_1^+. (b) $T = 0$ dot occupancies relative to half filling vs ε_1, with a vertical dashed line at $\varepsilon_1 = \varepsilon_1^+$. Inset: Evolution of the Kondo scale showing a linear dependence on $\Delta\varepsilon_1 = \varepsilon_1 - \varepsilon_1^+$.

A. Noninteracting dot 2

In the special case $U_2 = 0$, it is possible to integrate out the dot-2 degrees of freedom, thereby mapping the double-dot setup to an effective one-impurity Anderson model[7] in which the interacting dot 1 hybridizes with a conduction band described by a density of states

$$\rho_{\rm eff}(\varepsilon) \simeq \frac{1}{2D}\,\frac{(\varepsilon - \varepsilon_2)^2}{(\varepsilon - \varepsilon_2)^2 + \Gamma_2^2} \qquad (6)$$

for $|\varepsilon| \ll D$. For $\varepsilon_2 \neq 0$, $\rho_{\rm eff}(0)$ is nonzero and the dot-1 degree of freedom is completely quenched at sufficiently low temperatures. For $\varepsilon_2 = 0$, however, $\rho_{\rm eff}(\varepsilon)$ vanishes quadratically at $\varepsilon = 0$, leading to a realization of the pseudogap Anderson model.[7,8] In the mapped problem, the free-moment phase can be interpreted as a region of parameter space in which the loss of band states near the Fermi energy prevents Kondo screening of the dot-1 spin.

This subsection reports results of calculations performed directly on the double-dot model [Eq. (1)] with $U_2 = 0$. As found previously in studies of the mapped problem,[7,8] the free-moment phase is restricted to $\varepsilon_2 = 0$, $\varepsilon_1^- < \varepsilon_1 < \varepsilon_1^+$ [$\varepsilon_1^{\pm}(0,0)$ being denoted by filled circles in Figs. 2(a,d)]. Figure 3(a) shows the temperature variation of $\chi_{\rm imp}$, the contribution of the two dots ("impurities") to the magnetic susceptibility (defined and calculated in the usual way[25]), for several values of ε_1 along path OA in Figs. 2(a,d). In the free-moment phase (*e.g.*, $\varepsilon_1 = -\frac{1}{2}U_1$), a doublet ground state survives down to $T = 0$ with $T\chi_{\rm imp} = \frac{1}{4}$, characteristic of a free spin-$\frac{1}{2}$. In the strong-coupling phase (*e.g.*, $\varepsilon_1 = -U_1/125$), the system instead has a singlet ground state and $\chi_{\rm imp}$ (not just $T\chi_{\rm imp}$) vanishes as $T \to 0$. For ε_1 close to ε_1^+, singlet and doublet ground states are quasi-degenerate and $T\chi_{\rm imp} \approx \frac{1}{6}$ within a window of temperatures above some T^*; for $T \lesssim T^*$, there is a crossover to the low-temperature behavior of one or other phase. The crossover scale T^* vanishes continuously on approach to the phase boundary from either side, and at $\varepsilon_1 = \varepsilon_1^+$, $T\chi_{\rm imp} = \frac{1}{6}$ down

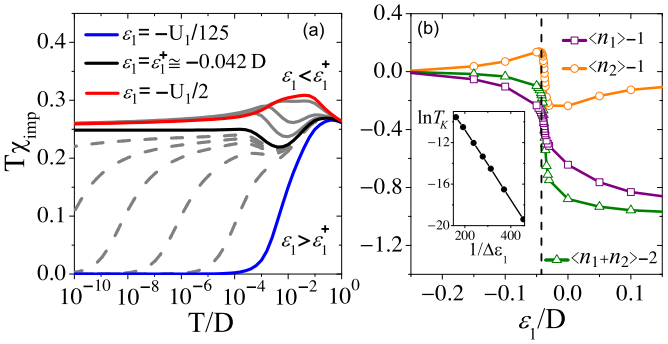

FIG. 4: (Color online). Interacting dot 2, $U_2 = -2\varepsilon_2 = \Gamma_2$: (a) $T\chi_{\rm imp}$ vs T for various values of ε_1 spanning the QPT at ε_1^+. (b) $T = 0$ dot occupancies relative to half filling vs ε_1 with a vertical dashed line at $\varepsilon_1 = \varepsilon_1^+$. Inset: Evolution of the Kondo scale T_K, showing $\ln T_K \propto 1/\Delta\varepsilon_1$ where $\Delta\varepsilon_1 = \varepsilon_1 - \varepsilon_1^+$.

to $T = 0$. The inset to Fig. 3(b) shows that the Kondo temperature T_K—proportional to the crossover scale T^* in the strong-coupling phase, and defined via the standard condition[25] $T_K\chi_{\rm imp}(T_K) = 0.0701$—vanishes linearly with $\Delta\varepsilon_1 = \varepsilon_1 - \varepsilon_1^+$, as expected at a first-order level-crossing QPT.

Further insight into the QPTs at $\varepsilon_1 = \varepsilon_1^\pm(0,0)$ can be gained by examining the dot occupancies $\langle n_i \rangle$ at zero temperature. On approach to the QPT from either phase, the occupancies [Fig. 3(b)] increasingly deviate from the values for isolated dots. Both occupancies undergo a jump at $\varepsilon_1 = \varepsilon_1^+$. The magnitude of the jump in $\langle n_1 \rangle$ can be identified with the weight under a delta-function peak in the dot-1 spectral density that passes through the Fermi energy at the QPT.[8] The limiting values of $\langle n_1 \rangle$ and $\langle n_2 \rangle$ on either side of the phase boundary, as well as the magnitudes of the jumps at the QPT, are found to change significantly with U_1, Γ_1, and Γ_2. However, the combined occupancy $\langle n_1 + n_2 \rangle$ for $\varepsilon_2 = 0$ in all cases remains very close to 2 throughout the free-moment phase, to 1 for all $\varepsilon_1 > \varepsilon_1^+$, and to 3 for all $\varepsilon_1 < \varepsilon_1^-$.

In order to understand this striking behavior of $\langle n_1 + n_2 \rangle$, it is useful to consider the wide-band limit in which D greatly exceeds all other energy scales. Here, $\langle n_1 + n_2 \rangle$ becomes identical to $n_{\rm imp} \equiv \langle N \rangle - \langle N \rangle_0$, where $\langle N \rangle$ ($\langle N \rangle_0$) is the total number of electrons with (without) the dots.[10] One can find $n_{\rm imp}$ using the aforementioned mapping to a one-impurity pseudogap Anderson model, valid for $U_2 = \varepsilon_2 = 0$. In the free-moment phase of the pseudogap model, particle-hole asymmetry is irrelevant[20] so $n_{\rm imp}(T = 0) = 2$; by contrast, particle-hole asymmetry is relevant in the strong-coupling phase,[20] forcing $n_{\rm imp}(T = 0) = 1$ or 3 depending on the sign of $\delta_1 \equiv \varepsilon_1 + \frac{1}{2}U_1$. These observations explain the near-pinning of $\langle n_1 + n_2 \rangle$ away from the wide-band limit, where $\langle n_1 + n_2 \rangle$ only approximately equals $n_{\rm imp}$. They also identify the differing response to particle-hole asymmetry in the two phases as the underlying reason for the first-order nature of the $U_2 = 0$ QPTs.

B. Weakly interacting dot 2

Now we turn to the case $U_2 = \Gamma_2$ representative of the crossover from a resonant dot 2 to an interacting one. The mapping to an effective one-impurity model breaks down for $U_2 \neq 0$, so the full double-dot model must be solved directly.

Figure 4(a) plots $T\chi_{\rm imp}$ vs T at different points along path O′A′ in Fig. 2(b). Deep in the strong-coupling phase (*e.g.*, $\varepsilon_1 = -U_1/125$) the system passes with decreasing temperature directly from a local-moment regime ($T\chi_{\rm imp} = \frac{1}{4}$) to the strong-coupling limit ($\rm T\chi_{imp} = 0$); just as for $U_2 = 0$, $\chi_{\rm imp}(T = 0) = 0$. For ε_1 just above ε_1^+ [*e.g.*, uppermost dashed line in Fig. 4(a)], $T\chi_{\rm imp}$ instead evolves with decreasing T from near $\frac{1}{4}$ towards the value $\frac{1}{6}$ characterizing the $U_2 = 0$ QPT (a tendency seen more clearly[24] for $0 < U_2 \ll \Gamma_2$), then rises and reaches a plateau near $\frac{1}{4}$ before finally decreasing to zero. The manner in which $T\chi_{\rm imp} \to 0$ as $T \to 0$ is identical to that in the Kondo regime of the conventional Anderson model,[25] with $\chi_{\rm imp}(T = 0) \simeq 0.1/T_K$ and T_K varying exponentially with $1/(\varepsilon_1 - \varepsilon_1^+)$ [inset to Fig. 4(b)]. For $\varepsilon_1 < \varepsilon_1^+$, $T\chi_{\rm imp}$ approaches the free-moment value $\frac{1}{4}$ from above, but there is no temperature scale that vanishes on approach to the phase boundary. These behaviors are all indicative of the Kosterlitz-Thouless nature of the QPT, which holds for any $U_2 > 0$ (with the sole exception of the first-order QPTs that arise from parity conservation in the special case of two identical Kondo-regime dots[10]). Like the ferromagnetic Kondo model, whose properties it closely parallels, the small-U_2 free-moment phase exhibits singular Fermi liquid behavior with a quasiparticle density of states that diverges at the Fermi energy.[21,26]

The dot occupancies for $U_2 = \Gamma_2$ [Fig. 4(b)] show generally the same trends vs ε_1 as found for $U_2 = 0$ [Fig. 3(b)], with the significant difference that there are no jumps. Since particle-hole asymmetry is a marginal perturbation in the conventional Anderson model,[25] $n_{\rm imp}(T = 0)$ varies continuously with ε_1, and there is no pinning of $\langle n_1 + n_2 \rangle$ in either phase.

Comparison between Figs. 3 and 4 shows that for $U_2 \lesssim \Gamma_2$, the properties retain their $U_2 = 0$ pseudogap character provided that the system is sufficiently far from the location $T = 0$, $\varepsilon_1 = \varepsilon_1^\pm$ of the QPT. With decreasing U_2 (not shown), the pseudogap behavior progressively extends to lower temperatures and/or smaller $|\varepsilon_1 - \varepsilon_1^\pm|$.

The physical property most likely to be accessible in experiments is the electrical conductance between the left and right leads. Figure 5(a) shows the linear conductance g [Eq. (5)] as a function of ε_1 for $U_2 = \Gamma_2$, $T = 0$, and four values of ε_2. Deep in the free-moment phase (around $\varepsilon_i = -\frac{1}{2}U_i$), dot 1 is in Coulomb blockade and since there is no Kondo effect and hence no Kondo resonance, transport takes place solely through dot 2. For fixed ε_1 near $-\frac{1}{2}U_1 = -0.25D$, the zero-temperature conductance decreases from its unitary limit $g = 2e^2/h$ as ε_2 is varied from $-\frac{1}{2}U_2$ (squares) to higher (circles and diamonds) or

lower values, while for fixed ε_2 near $-\frac{1}{2}U_2$, the system passes through a QPT at $\varepsilon_1 = \varepsilon_1^{\pm}$, where g undergoes a jump. For ε_1 right above ε_1^+ or right below ε_1^-, there is a Kondo effect centered primarily on dot 1, and interference between transport through the two dots causes g to decrease abruptly. On moving deeper into the strong-coupling phase, the dot-1 occupancy moves further from unity, interference from transport through dot 1 is reduced, and g rises again. The preceding picture holds until dot 2 becomes sufficiently particle-hole asymmetric that the strong-coupling phase spans all values of ε_1, and g vs ε_1 shows no sign of any QPT [triangles in Fig. 5(a)].

The conductance signatures of the QPT persist to $T > 0$, as illustrated in Fig. 5(b), which plots g vs ε_1 for $U_2 = \Gamma_2$, $\varepsilon_2 = 0.075U_2$, and three temperatures specified in the caption as multiples of $T_{K0} = 7 \times 10^{-4} D$: the Kondo scale when dot 2 is isolated ($\Gamma_2 = 0$) and dot 1 is at particle-hole symmetry ($\varepsilon_1 = -\frac{1}{2}U_1$). The foremost effect of increasing T is a progressive suppression of the Kondo effect, leading to a smoothing and weakening of the conductance dips in the vicinity of the QPTs, as well as shifts in positions of the local minima in g to larger values of $|\varepsilon_1 + \frac{1}{2}U_1|$.

IV. WEAK VERSUS STRONG DOT-2 INTERACTIONS

In this section, we compare the regime $U_2 \lesssim \Gamma_2$ described above with the one $U_2 \gg \Gamma_2$ studied in most previous work on Kondo physics in parallel double quantum dots. We show that these regimes have very different spin correlations between the different components of the double-quantum-dot device. Furthermore, the regimes can be distinguished experimentally through linear conductance measurements.

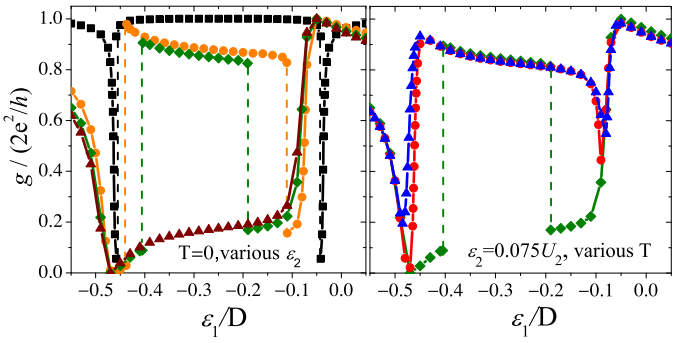

FIG. 5: (Color online). Linear conductance g vs ε_1 for $U_2 = \Gamma_2$. Left: Temperature $T = 0$ and scaled dot-2 level energies $\varepsilon_2/U_2 = -0.5$ (■), 0 (●), 0.075 (♦), and 0.11 (▲). Right: $\varepsilon_2 = 0.075U_2$ and scaled temperatures $T/T_{K0} = 0$ (♦), 0.0057 (●), and 0.228 (▲).

A. Spin correlations

Insight into the connection between the regimes of small and large U_2/Γ_2 can be gained from the static spin-spin correlation $\langle \mathbf{S}_i \cdot \mathbf{S}_{\rm leads} \rangle$ between dot i and the leads, as well as from the interdot correlation $\langle \mathbf{S}_1 \cdot \mathbf{S}_2 \rangle$. Here, $\mathbf{S}_i = \frac{1}{2}\sum_{\sigma,\sigma'} d^\dagger_{i\sigma} \boldsymbol{\sigma}_{\sigma,\sigma'} d_{i\sigma'}$ and $\mathbf{S}_{\rm leads} = \frac{1}{2}\sum_{j,\mathbf{k},\mathbf{k}',\sigma,\sigma'} c^\dagger_{j\mathbf{k}\sigma} \boldsymbol{\sigma}_{\sigma,\sigma'} c_{j\mathbf{k}'\sigma'}$, where $\boldsymbol{\sigma}$ is a vector of Pauli matrices.

Figure 6 shows the $T = 0$ spin-spin correlations vs U_2/Γ_2 for fixed $\Gamma_2 = 0.02D$ with both dots at particle-hole symmetry, *i.e.*, at the center of the free-moment phase.[27] For $U_2 = \varepsilon_2 = 0$, spin-0 and spin-$\frac{1}{2}$ configurations of dot 2 should be equally probable, whereas dot 1 is expected to have a well-defined spin-$\frac{1}{2}$ at low temperatures. The facts that $\langle \mathbf{S}_1 \cdot \mathbf{S}_{\rm leads} \rangle$ is much smaller in magnitude than $\langle \mathbf{S}_2 \cdot \mathbf{S}_{\rm leads} \rangle$, and that the latter quantity is close to the value $\frac{1}{2} \times (-\frac{3}{4}) = -\frac{3}{8}$ it would take if dot 1 were absent from the system, indicate that for $U_2 = 0$ the residual spin-$\frac{1}{2}$ degree of freedom is located primarily on dot 1, which is almost decoupled from other parts of the system.

Increasing U_2 enhances the magnetic character of dot 2 and so strengthens both the dot's antiferromagnetic correlation with the leads and (via an effective RKKY interaction[6,10]) its ferromagnetic correlation with dot 1. There is an even more pronounced growth in the antiferromagnetic correlation between dot 1 and the leads. These trends continue until U_2/Γ_2 becomes of order 5, by which point each dot carries a well-defined spin-$\frac{1}{2}$. To good approximation, these spins combine to form a triplet that is partially Kondo-screened by the leads, to yield a strongly entangled spin-$\frac{1}{2}$ ground state.[10,18] Since the effective exchange interaction between dot 2 and the leads is proportional[6] to $1/U_2$, further increase of U_2/Γ_2 beyond about 5 results in a gradual reduction in the magnitudes of both $\langle \mathbf{S}_1 \cdot \mathbf{S}_{\rm leads} \rangle$ and $\langle \mathbf{S}_1 \cdot \mathbf{S}_2 \rangle$.

B. Transport properties

Although the regimes $U_2 \ll \Gamma_2$ and $U_2 \gg \Gamma_2$ feature very different spin correlations, they belong to the same phase and therefore have qualitatively the same asymptotic low-temperature properties.[26] The question remains whether the two regimes may be distinguished through their behavior at higher T.

Figure 7(a) shows g vs T at the particle-hole-symmetric point $\varepsilon_i = -\frac{1}{2}U_i$ for six values of U_2. For $U_2 \gg \Gamma_2$, the conductance drops significantly below its unitary limit once the temperature rises above the characteristic scale $T_K^{S=1}$ of the spin-1 Kondo effect, which is[10] of order T_{K0}. For $U_2 \lesssim \Gamma_2$, there is no Kondo physics in the free-moment phase and g remains close to $2e^2/h$ up to much higher temperatures of order Γ_2.

Figure 7(b) plots g vs ε_1 at different temperatures for $U_2 = -2\varepsilon_2 = \Gamma_2$ (path O′A′ in Fig. 2) and for

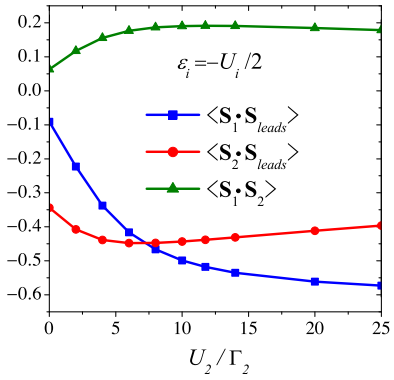

FIG. 6: (Color online). Dot-lead and dot-dot spin correlations vs scaled interaction strength U_2/Γ_2, determined at zero temperature for level energies $\varepsilon_i = -\frac{1}{2}U_i$, *i.e.*, at the center of the free-moment phase. Increasing U_2 from zero enhances the entanglement between dot 1 and the other parts of the system as the residual spin-$\frac{1}{2}$ degree of freedom evolves from being localized on dot 1 (for $U_2 = 0$) to being distributed throughout the system (for $U_2 \gg \Gamma_2$).

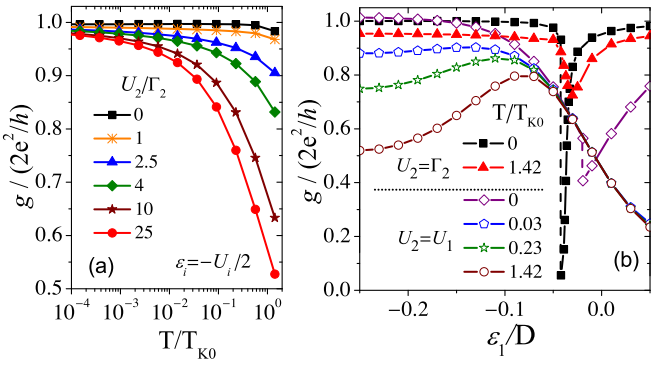

FIG. 7: (Color online). Conductance g plotted (a) vs T at particle-hole symmetry ($\varepsilon_i = -\frac{1}{2}U_i$); and (b) vs ε_1 for $\varepsilon_2 = -\frac{1}{2}U_2$, comparing the local-moment and underscreened spin-1 Kondo regimes of the free-moment phase, represented by $U_2 = \Gamma_2$ and $U_2 = U_1$, respectively.

$U_2 = -2\varepsilon_2 = U_1$ (path O″A″). Just as in Fig. 7(a), the T dependence of the conductance in the free-moment phase is much weaker for $U_2 \lesssim \Gamma_2$ than for $U_2 \gg \Gamma_2$. Near particle-hole symmetry ($\varepsilon_1 = -0.25D$), the latter regime has $d^2g/d\varepsilon_1^2 > 0$ at all but the very lowest temperatures, reflecting the ε_1 dependence[10] of $T_K^{S=1}$, whereas $d^2g/d\varepsilon_1^2 \leq 0$ in the local-moment case.

Similar trends to those shown in Fig. 7 are found for other choices of ε_1 and ε_2 that place the system in the free-moment phase. We conclude that the local-moment and underscreened spin-1 Kondo regimes can be clearly differentiated via their conductance at temperatures (of order the typical Kondo scale T_{K0}) that should be readily attainable in experiments.

V. SUMMARY

We have studied two quantum dots coupled in parallel to metallic leads, focusing on situations where "dot 2" has a weaker on-site Coulomb interaction than "dot 1": $U_2 < U_1$. For $U_2 \lesssim \Gamma_2$, the tunneling width of the dot-2 level, the properties still reflect the pseudogap Kondo physics found previously for $U_2 = 0$. For all $U_2 > 0$, Kondo-screened and free-moment phases are separated by quantum phase transitions of the Kosterlitz-Thouless type that have signatures in the electrical conductance up to experimentally accessible temperatures.

In the free-moment phase, conductance measurements can also distinguish the small-U_2 regime, in which dot 1 carries a spin-$\frac{1}{2}$ and is essentially disconnected from the rest of the system, from the regime $U_2 \gg \Gamma_2$ in which both dots contain strong electron correlations and their combined spin is partially screened by the leads. Given the feasibility of tuning between these two cases—and of crossing into the Kondo phase (above an underlying zero-temperature transition)—by adjusting just one gate voltage on each dot, this system offers fascinating possibilities for controlled experimental study of quantum phase transitions and of variations in the strength and spatial distribution of entanglement in singular Fermi liquids.

Acknowledgments

We thank D. Logan for helpful discussions. This work was supported by NSF DMR Grants 0710540, 0710581, 1107814, and 1108285 in the United States, and by CNPq and by FAPESP Grant 2010/20804-9 in Brazil.

[1] L. Kouwenhoven and L. Glazman, Phys. World **14**, 33 (2001).
[2] H. Jeong, A. M. Chang, and M. R. Melloch, Science **293**, 2221 (2001); J. C. Chen, A. M. Chang, and M. R. Melloch, Phys. Rev. Lett. **92**, 176801 (2004); N. J. Craig, J. M. Taylor, E. A. Lester, C. M. Marcus, M. P. Hanson, and A. C. Gossard, Science **304**, 565 (2004); A. Hübel, K. Held, J. Weis, and K. v. Klitzing Phys. Rev. Lett **101**, 186804 (2008).
[3] R. M. Potok, I. G. Rau, H. Shtrikman, Y. Oreg and D. Goldhaber-Gordon, Nature (London) **446**, 167 (2007).
[4] W. Hofstetter and H. Schoeller, Phys. Rev. Lett. **88**, 016803 (2001).
[5] Y. Oreg and D. Goldhaber-Gordon, Phys. Rev. Lett. **90**, 136602 (2003); M. Pustilnik, L. Borda, L. I. Glazman, and J. von Delft, Phys. Rev. B **69**, 115316 (2004); M. R. Galpin, D. E. Logan, and H. R. Krishnamurthy, Phys. Rev. Lett **94**, 186406 (2005).
[6] R. Žitko and J. Bonča, Phys. Rev. B **74**, 045312 (2006).
[7] L. G. G. V. Dias da Silva, N. P. Sandler, K. Ingersent, and

S. E. Ulloa, Phys. Rev. Lett. **97**, 096603 (2006).
[8] L. G. G. V. Dias da Silva, K. Ingersent, N. Sandler, and S. E. Ulloa, Phys. Rev. B **78**, 153304 (2008).
[9] L. G. G. V. Dias da Silva, N. Sandler, P. Simon, K. Ingersent, and S. E. Ulloa, Phys. Rev. Lett. **102**, 166806 (2009).
[10] D. E. Logan, C. J. Wright, and M. R. Galpin, Phys. Rev. B **80**, 125117 (2009).
[11] S. Tarucha, D. G. Austing, Y. Tokura, W. G. van der Wiel, and L. P. Kouwenhoven, Phys. Rev. Lett. **84**, 2485 (2000).
[12] A. Kogan, G. Granger, M. A. Kastner, D. Goldhaber-Gordon, and H. Shtrikman, Phys. Rev. B **67**, 113309 (2003).
[13] W. G. van der Wiel, S. De Franceschi, J. M. Elzerman, S. Tarucha, L. P. Kouwenhoven, J. Motohisa, F. Nakajima, and T. Fukui, Phys. Rev. Lett. **88**, 126803 (2002).
[14] M. Eto and Y. V. Nazarov, Phys. Rev. Lett. **85**, 1306 (2000); M. Pustilnik and L. I. Glazman, *ibid.* 2993 (2000); R. López, R. Aguado, and G. Platero, Phys. Rev. Lett. **89**, 136802 (2002); M. Pustilnik, L. I. Glazman, and W. Hofstetter, Phys. Rev. B **68**, 161303(R) (2003).
[15] M. Vojta, R. Bulla, and W. Hofstetter, Phys. Rev. B **65**, 140405 (2002).
[16] D. Boese, W. Hofstetter, and H. Schoeller, Phys. Rev. B **66**, 125315 (2002); C. A. Büsser, G. B. Martins, K. A. Al-Hassanieh, A. Moreo, and E. Dagotto, *ibid.* **70**, 245303 (2004); G.-H. Ding, C. K. Kim, and K. Nahm *ibid.* **71**, 205313 (2005); Y. Tanaka and N. Kawakami, *ibid.* **72**, 085304 (2005).
[17] R. López, D. Sánchez, M. Lee, M.-S. Choi, P. Simon, and K. LeHur, Phys. Rev. B **75**, 115312 (2005); Y. Tanaka and N. Kawakami, J. Phys. Soc. Jpn. **75**, 015004 (2006).
[18] P. Nozières and A. Blandin, J. Phys. (Paris) **41**, 193 (1980); A. Posazhennikova and P. Coleman, Phys. Rev. Lett. **94**, 036802 (2005); P. Roura Bas and A. A. Aligia, Phys. Rev. B **80**, 035308 (2009).
[19] D. Withoff and E. Fradkin, Phys. Rev. Lett. **64**, 1835 (1990); K. Chen and C. Jayaprakash, J. Phys.: Condens. Matter **7**, L491 (1995); R. Bulla, T. Pruschke, and A. C. Hewson, *ibid.* **9**, 10 463 (1997).
[20] K. Ingersent, Phys. Rev. B **54**, 11936 (1996); C. Gonzalez-Buxton and K. Ingersent, *ibid.* **57**, 14 254 (1998).
[21] P. Mehta, N. Andrei, and P. Coleman Phys. Rev. B **72**, 014430 (2005); W. Koller, A. Hewson, and D. Meyer, *ibid.* 045117 (2005).
[22] Y. Meir and N. S. Wingreen, Phys. Rev. Lett. **68**, 2512 (1992).
[23] R. Bulla, T. Costi, and T. Pruschke, Rev. Mod. Phys. **80**, 395 (2008).
[24] Preliminary results for the $U_2 > 0$ phase diagram, susceptibility, and zero-temperature conductance appeared in W. B. Lane, Ph.D. thesis, University of Florida, 2008.
[25] H. R. Krishna-murthy, J. W. Wilkins and K. G. Wilson, Phys. Rev. B **21**, 1003 (1980); *ibid.* 1044 (1980).
[26] Analysis of the scattering phase shifts indicates that the free-moment phase exhibits singular Fermi liquid behavior for all $U_2 > 0$.
[27] Within the numerical renormalization-group (NRG) approach, the spin of the leads is calculated as $\mathbf{S}_{\rm leads} = \frac{1}{2}\sum_{n=0}^{N}\sum_{\sigma,\sigma'} f^\dagger_{n\sigma}\boldsymbol{\sigma}_{\sigma,\sigma'}f_{n\sigma'}$ where $f_{n\sigma}$ annihilates an electron of spin z component σ on site n of the linear chain resulting[23] from the logarithmic discretization of $H_{\rm leads}$ [Eq. (2)]. The correlations plotted in Fig. 6 are limiting values for high NRG iteration numbers N corresponding to temperatures $T \to 0$.